1

Polarimetry with ASTRO-H Soft Gamma-ray Detector

Hiroyasu Tajima (KIPAC, Stanford University)

Shin'ichiro Takeda (Institute for Space and Astronautical Science, JAXA)

ASTRO-H SGD team[1]

Abstract

ASTRO-H is a next generation JAXA X-ray satellite to be launched in 2014. Soft Gamma-ray Detector (SGD) onboard ASTRO-H is a semiconductor Compton camera with a narrow field-of-view (FOV) to achieve very low background. Although the SGD is primarily a spectrometer in the 40–600 keV energy band, it is also sensitive to polarization in the 50–200 keV energy band. This paper describes instrument design, expected performance, and experimental validation of polarimetric performance of the SGD.

1.1 Introduction

ASTRO-H, the new Japanese X-ray Astronomy Satellite(1) following Suzaku, is a combination of high energy-resolution soft X-ray spectroscopy (0.3–10 keV) provided by thin-foil X-ray optics (SXT, Soft X-ray Telescope) and a microcalorimeter array (SXS, Soft X-ray Spectrometer), soft X-ray imaging spectroscopy (0.5–12 keV) provided by SXT and CCD (SXI, Soft X-ray Imager), hard X-ray imaging spectroscopy (3–80 keV) provided by multilayer coating, focusing hard X-ray mirrors (HXT, Hard X-ray Telescope) and silicon (Si) and cadmium telluride (CdTe) cross-strip detectors (HXI, Hard X-ray Imager)(2), and soft gamma-ray spectroscopy (40–600 keV) provided by semiconductor Compton camera with narrow FOV (SGD, Soft Gamma-ray Detector)(3). The SXT-SXS and SGD systems will be developed by international collaboration led by Japanese and US institutions.

The SXS will use a 6×6 format microcalorimeter array. The energy resolution is expected to be better than 7 eV. The field of view and the effective area will be, respectively, about 3 arc minutes and about 210 cm^2 combined with the ∼6 m focal-length SXT. The SXT-SXS system will provide accurate measurements of the temperature and the turbulence/macroscopic motions in distant clusters up to redshift of about 1, allowing studies of

the formation history of the large scale structure of the universe, which will eventually constrain the evolution of the dark energy.

The focal length of the HXT will be 12 m and the effective area will be larger than 200 cm^2 at 50 keV. The HXI utilizes four layers of double-sided Si strip detectors overlaid on a double-sided CdTe strip detector with a BGO ($Bi_4Ge_3O_{12}$) active shield. The extremely low background of the HXT-HXI system will improve the sensitivity in 20–80 keV range by almost two orders of magnitude, compared to conventional non-imaging detectors in this energy band. Search for highly absorbed active galactic nuclei and understanding their evolution is one of main science topics of the HXT-HXI.

The SGD also utilizes semiconductor detectors such as Si and CdTe pixel detectors with fine energy resolution (<2 keV). Narrow FOV constrained by BGO active shield combined with good background rejection by Compton kinematics will improve the sensitivity by an order of magnitude in 40–600 keV band compared with the currently operating instruments in Space. The SGD will allows us to study soft gamma-ray emissions from ∼100 of AGNs, 511 keV emissions from galactic sources, and polarization from sources with >a few×1/100 brightness of Crab.

The ASTRO-H mission is an official JAXA project and in the phase-B development as of 2009. We expect to launch it in 2014.

1.2 SGD Instrument Design

The SGD is a Compton telescope with narrow FOV, which provides a constraint on Compton kinematics to enhance its background rejection capabilities. The SGD instrument is divided into two units that are mounted on the opposite sides of the space craft for better weight balance. Each unit is consist of a 4×1 array of identical Compton camera modules surround by BGO shield units and fine passive collimators. Figure 1.1 (a) shows a conceptual drawing of the SGD unit. A BGO collimator defines 10° FOV of the telescope for high energy photons while a fine collimator restricts the FOV to 0.5° for low energy photons (<150∼300 keV), which is essential to minimize the CXB (cosmic X-ray backgrounds) and source confusions. Scintillation light from the BGO crystals is detected by avalanche photo-diodes (APDs) allowing a compact design compared with phototubes.

The hybrid design of the Compton camera module, illustrated in Figure 1.1 (b), incorporates both pixelated Si and CdTe detectors. The Si layers enhance efficiencies below ∼300 keV, and also improve the angular resolution because of smaller effect from the finite momentum of the Compton-scattering electrons (Doppler broadening) than CdTe. The Compton camera

consists of 32 layers of Si sensors and 8 layers of CdTe sensors surrounded by 2 layers of CdTe sensors. The thickness is 0.6 mm for Si and 0.75 mm for CdTe mainly to reduce risks associated high bias voltages required by a thicker sensors which is preferred for higher interaction probability. The pixel size is 3.2×3.2 mm^2 for both Si and CdTe to optimize the angular resolution of the Compton kinematics and the number of channels required. The geometrical acceptance area of each Compton camera is 5.12×5.12 cm^2.

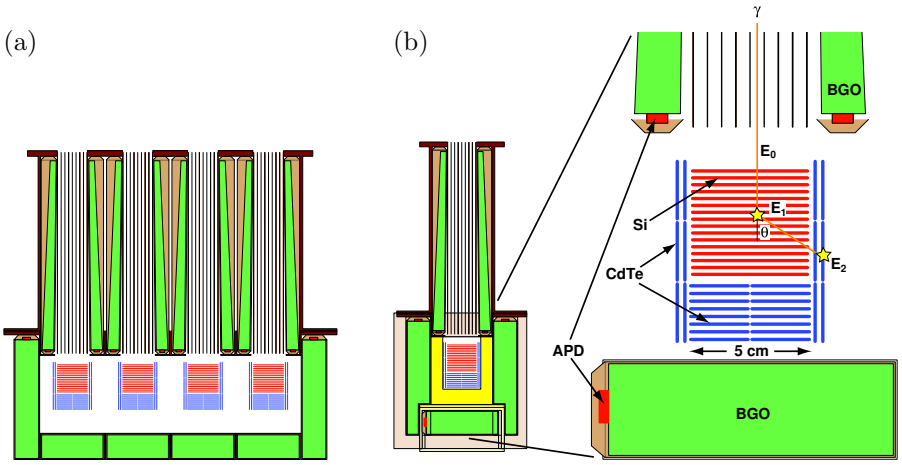

Fig. 1.1. Conceptual drawing of (a) an SGD instrument and (b) an SGD Compton camera unit.

We require each SGD event to interact twice in a Compton camera, once by Compton scattering in a Si sensor, and then by photo-absorption in a CdTe sensor. Once the locations and energies of the two interactions are measured as shown in Figure 1.1 (b), the Compton kinematics allows us to calculate the direction of the incident photon using the formula,

$$\cos\theta \;=\; 1+\frac{m_e c^2}{E_2+E_1}-\frac{m_e c^2}{E_2}, \tag{1.1}$$

where θ is the polar angle of the Compton scattering, and E_1 and E_2 are the energy deposited in each photon interaction. The high energy resolution of the Si and CdTe devices is essential to reduce the uncertainty of θ. The angular resolution is limited to $\sim8^\circ$ at 100 keV and $\sim3^\circ$ at 600 keV due to the Doppler broadening. We require that the incident photon angle inferred from the Compton kinematics is consistent with the FOV, which dramatically reduces dominant background sources such as radio-activation of the detector materials and neutrons. Low backgrounds realized by the Compton kinematics is the key feature of the SGD since the photon sensitivity of the the SGD is limited by the backgrounds, not the effective area.

As a natural consequence of the Compton approach used to decrease backgrounds, the SGD is quite sensitive to X/γ-ray polarization, thereby opening up a new window to study the geometry of the particle acceleration and emission regions in compact objects and astrophysical jets. In addition, detection of the polarization from cosmological distances (like AGNs in flare states) can set stringent constraints on models of the Lorentz-invariance violation. Detection of the polarization signature caused by the propagation of X-rays through the Kerr space-time of stellar mass black holes can also test Einstein's theory of General Relativity.

The Compton scattering cross section depends on the azimuth Compton scattering angle with respect to the incident polarization vector as;

$$\frac{\delta\sigma}{\delta\Omega} \propto \left(\frac{E'_\gamma}{E_\gamma}\right)^2 \left(\frac{E'_\gamma}{E_\gamma} + \frac{E_\gamma}{E'_\gamma} - 2\sin^2\theta \cdot \cos\phi\right), \tag{1.2}$$

where ϕ and θ are the azimuth and polar Comton scattering angles, and E_γ and E'_γ are incident and scattered photon energies. It shows that the ϕ modulation is largest at $\theta = 90°$, *i.e.* parpendicular to the incident direction.

1.3 Expected Performance

Effective area, polarization sensitivity and non X-ray backgrounds are evaluated by Geant4-based Monte Carlo simulations. The solid line in Figure 1.2 (a) shows the effective area as a function of the incident energy. Maximum effective area of more than 30 cm^2 is realized at around 80–100 keV, which corresponds to $\sim$15% reconstruction efficiency since the geometrical area of the SGD is 210 cm^2. The effective area at low energies is suppressed due to the photo-absorption in Si while the loss at high energies is due to multiple-Compton events, which can be recovered by improved reconstruction algorithm. The dotted line in Figure 1.2 (a) shows the inverse of minimum detectable polarization (MDP) in arbitray unit assuming no background. The polarization sensitivity falls off slower at low energies and faster at high energies due to lower modulation factor resulting from more forward scattering at higher energies. This result indicates that the SGD is sensitive to the polarization in the 50–200 keV energy band.

Main in-orbit background components of the SGD are expected to be activations induced during the SAA and elastic scatterings of albedo neutrons, at the expected orbit of ASTRO-H (altitude of 550 km with an inclination angle of 31°). These background events can be heavily suppressed by a combination of multi-layer configuration, active shield, and the background rejection based on the Compton kinematics. The remaining background

level is estimated to be much lower than any past instrument as shown in Figure 1.2 (b). The neutron background (green dotted curve) is estimated by the simulation assuming the neutron spectrum described in Ref. (4). The flux of the neutron background is scaled by a factor of two based on the background studies of the Suzaku hard X-ray detector (5). The spectrum of the activation background (blue dashed curve) is estimated from experimental results on the radioactivities induced by monoenergetic protons (6). The flux is scaled by a rejection factor expected from Compton kinematics constraints. The signal fluxes corresponding to 1/100 and 1/1000 of the Crab brightness are overlaid in black and orange dotted straight lines, respectively. This clearly illustrates that the expected background in the SGD varies from 1/1000 to 1/100 of the Crab brightness in the 50–200 keV band.

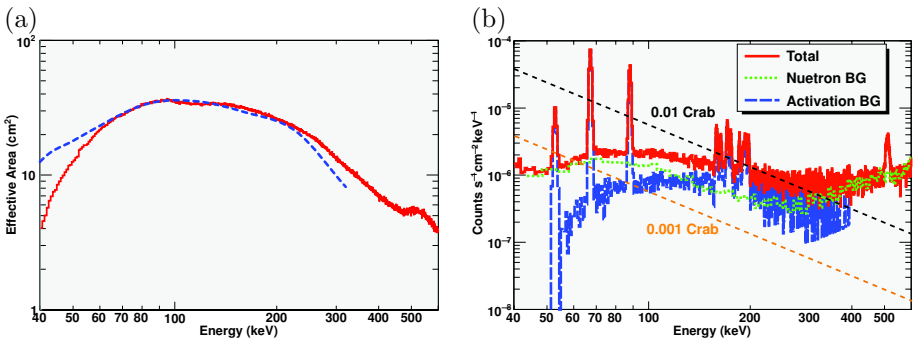

Fig. 1.2. (a) Effective area as a function of incident energy. (b) Background flux as a function of reconstructed energy.

The polarization signature of incident gamma-ray is detected by the modulation of the azimuth angle distribution of Compton scattering in the SGD as shown in Figure 1.3 (a) for a 100%-polarized source. A fit to $AVG[1 + Q\cos 2(\phi - \chi_0)]$ yields $Q = 56.7 \pm 1.0\%$, where Q is the modulation factor which is proportional to the polarization degree and χ_0 is the angle of the polarization vector. Using the modulation factor obtained here and the background level described above, we can calculate the MDP analytically assuming no systematic effect from uneven backgrounds and detector response. Figure 1.3 (b) shows the 3σ MDP as a function of the observation time for sources with 1, 0.1 and 0.01 of the Crab brightness, which can be parametrized as $3.5\%\sqrt{10^4/t_{\rm obs}}$, $3.6\%\sqrt{10^5/t_{\rm obs}}$ and $4.3\%\sqrt{10^6/t_{\rm obs}}$, respectively, where $t_{\rm obs}$ is the observation time in seconds. We can conclude that the SGD can detect polarization from sources down to a few$\times$1/100 of the the Crab brightness with a polarization degree of several % in a few$\times$100 ks of observation time.

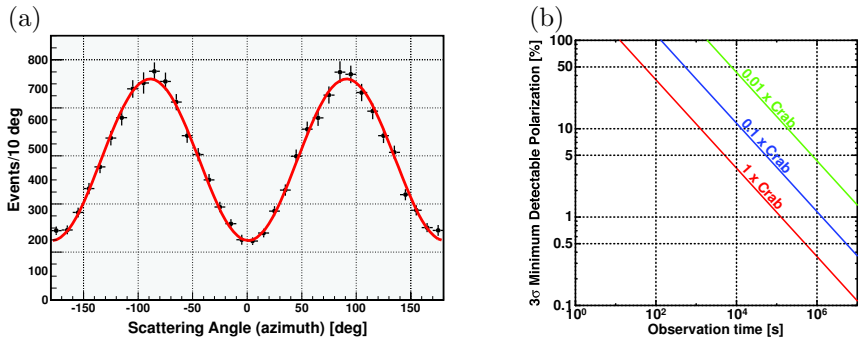

Fig. 1.3. (a) Efficiency-corrected azimuth angle distribution of Compton scattering from a source with a brightness of Crab and 100% linear polarization in a 10 ks observation. (b) 3σ MDP as a function of observation time for sources with 1, 0.1 and 0.01 of the Crab brightness.

1.4 Experimental Validation

Most polarimeters rotate instruments to minimize systematic effects which may arise from uneven detector responses. Since the SGD is primarily a spectrometer, it does not rotate the instrument to avoid complex mechanical design. Because of this, it is crucial to obtain correct azimuthal response of the instrument from the MC simulation. We plan to validate and calibrate the MC simulation using non-polarized astronomical sources and also using beam tests. As a demonstration of this validation and calibration process, we have performed a beam test of a prototype Compton camera using nearly 100%-polarized 250-keV beam at SPring-8 synchrotron photon facility.

The prototype Compton camera consists of one layer of Si sensor followed by four layers of CdTe sensors surrounded by one layer of CdTe sensors. The 250-keV synchrotron beam with 99.99% polarization is scattered in an aluminum block by 90° with a ∼3° acceptance window in order to shine the entire Si sensor surface. The resulting photon beam has an energy of ∼170 keV and a polarization degree of ∼92.5%. Detailed description of experimental setup and results is given elsewhere (7). Figure 1.4 (a) compares the experimental and simulation results of the azimuth angle distribution without any instrument response corrections. Note that dips at ±45° and ±135° are due to gaps at the four corner of the experimental setup. Figure 1.4 (b) shows the experimental azimuth angle distribution with instrument response corrections obtained from the MC simulation. A fit to the above formula yields $Q = 82.9 \pm 0.8\%$ while a similar procedure performed on the simulation yields $Q = 85.6 \pm 2.7\%$. This result validates our modeling of instrument geometry and response at ∼3% level.

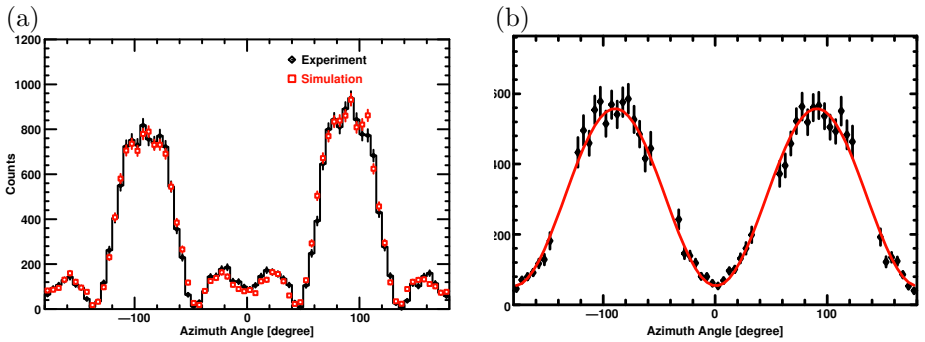

Fig. 1.4. (a) Comparison of experimental (black solid diamond) and simulation (red open square) results of the azimuth angle distribution without any instrument response corrections. (b) Experimental azimuth angle distribution with instrument response corrections obtained from the MC simulation with a model fit.

Since the SGD Compton camera is square shaped, measurements of polarization property may systematically depends on the polarization angle. Figure 1.5 shows (a) the modulation factor as a function of the polarization angle and (b) the difference between the polarization angle derived from the experimental data and that of the incident photons as a function of the incident polarization angle. Both plots show no visible systematic effect from the incident polarization angle.

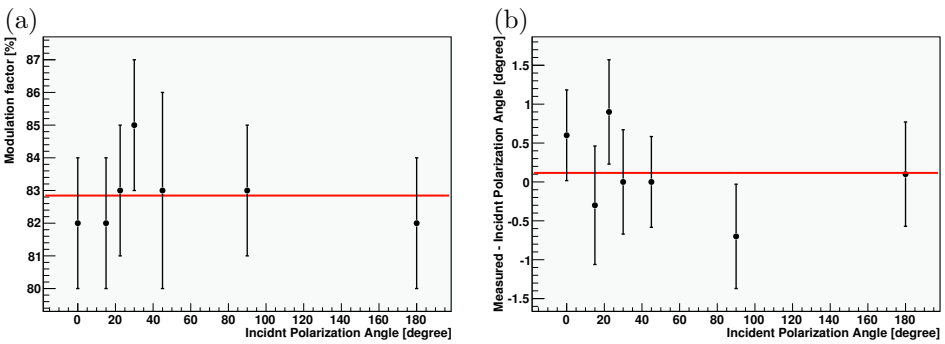

Fig. 1.5. (a) Modulation factor as a function of the polarization angle. (b) The difference between the polarization angle derived from the experimental data and that of the incident photons as a function of the incident polarization angle.

Fake polarization signature in the azimuth angle distribution for zero polarization sources degrades the polarization sensitivity of the instrument and also produces systematic effects on measurements of polarization properties. Such fake polarization may be caused by uneven instrument response, wrong modeling of the instrument response and/or uneven backgrounds. The ef-

fect of uneven backgrounds needs to be carefully studied using several faint sources with no expected polarization on orbit. Here we study the effect of uneven instrument response and its modeling by using unpolarized data synthesized from two samples of experimental data with orthogonal polarization. A fit to the synthesized data yields $Q = 3.0 \pm 1.5\%$, corresponding to an apparent polarization of $3.3 \pm 1.7\%$, which is comparable to uncertainties of the modulation factor (*i.e.* polrization degree) described above.

1.5 Summary

To summarize, the SGD onboard ASTRO-H will be very sensitive polarimeter in 50–200 keV band as well as the most sensitive spectrometer in 80–600 keV band after the expected launch in 2014. The SGD will be sensitive to $\lesssim$10% polarization for sources with several$\times$0.01 of the Crab brightness, which includes many Galactic sources and some AGNs in flare states. Since ASTRO-H is a general X-ray observatory, it will observe thousands of astronomical sources in its lifetime regardless of prospect for the polarization. Observations of many unpolarized sources with different degree of brightness allow us to calibrate the instrument response and to carefully study systematic effects from backgrounds. Observations of many sources also present opportunities for a great discovery of the polarization from unexpected sources.

Notes

1 ASTRO-H SGD team includes S. Nakahira, K. Yamaoka (Aoyama-gakuin University), K. Doutsu, K. Fukami, Y. Fukazawa, Y. Hanabata, K. Hayashi, K. Hiragi, M. Matsuoka, T. Mizuno, S. Nishino, Y. Umeki (Hiroshima University), T. Fukuyama, S. Ishikawa, J. Katsuta, M. Kokubun, M. Koseki, H. Odaka, S. Saito, C. Sasaki, R. Sato, S. Sugimoto, T. Takahashi, S. Watanabe (Institute for Space and Astronautical Science), T. Endo, J. Harayama, T. Kozu, M. Tashiro, Y. Terada, Y. Yaji (Saitama University) G. Madejski, T. Tanaka, Y. Uchiyama (Stanford University), T. Enoto, T. Kitaguchi, K. Makishima, K. Nakajima, K. Nakazawa, H. Nishioka, H. Noda, S. Torii, S. Yamada, T. Yuasa (University of Tokyo), J. Kataoka, T. Miura, M. Yoshino (Waseda University)

References

[1] T. Takahashi *et. al.*, Proc. SPIE **7011**, 14T (2008)
[2] M. Kokubun *et. al.*, Proc. SPIE **7011**, 21K (2008)
[3] H. Tajima *et. al.*, IEEE Trans. Nucl. Sci. **52**, 2749 (2005)
[4] T. W. Armstrong *et. al.*, J. Geophys. Res. **78**, 2715 (1973)
[5] Y. Fukazawa *et. al.* Pub. of Astro. Soc. of Japan **61**, S17 (2009)
[6] M. Murakami *et. al.*, IEEE Trans. Nucl. Sci. **50**, 1013 (2003).
[7] S. Takeda *et. al.* to be submitted to Nucl. Inst. and Meth. A.